Chemical Physics 58 (1981) 371–383
North-Holland Publishing Company

ORIGIN OF InI EMISSION IN LASER STUDIES OF THE CROSSED BEAM REACTION $In+I_2$

Charles T. RETTNER, Ludger WÖSTE,* and Richard N. ZARE
Department of Chemistry, Stanford University, Stanford, CA 94305, USA

Received 12 January 1981

When a beam of In is cross fired at a beam of I_2 and the intersection is irradiated by various cw laser sources, InI emission is observed. The origin of this emission is shown to be laser-induced fluorescence (LIF) from the ground state indium monoiodide product of the reaction $In+I_2 \rightarrow InI+I$, rather than laser-induced chemiluminescence (LIC) through the excitation of the I_2 reagent in the reaction $In+I_2^* \rightarrow InI^*+I$. An upper bound on the cross section for the later process is estimated to be $\leq 2.5\times10^{-16}$ cm^2. The LIF excitation spectrum reveals a strong inversion in the InI vibrational population distribution, with the fraction of the total excess energy of reaction in vibration exceeding 0.5. Preliminary results for the $Tl+I_2$ reaction system show the same LIF mechanism for the TlI emission.

1. Introduction

A previous study reported that intense metal monoiodide emission is obtained when an indium or thalium beam–iodine gas system is illuminated with the 514.5 nm line of an argon ion laser [1]. Since these metals are expected to react rapidly with molecular iodine [2], there are two obvious possibilities for the production of this emission. The laser may excite an iodine molecule prior to reaction, yielding an excited product. Alternatively, the laser light may be absorbed directly by the reaction product causing it to fluoresce. The former process is called laser-induced chemiluminescence (LIC) while the latter is called laser-induced fluorescence (LIF) [3, 4].

The resolved emission spectrum showed broad oscillations and extended over more than 100 nm [1], suggestive of a chemiluminescent process. Furthermore, the B–X system of I_2 is indeed strongly pumped by the 514.5 nm laser light. Thus an LIC mechanism was invoked and the polarization dependence of the emission was thought to reflect the orientation dependence of the $M+I_2^*$ reaction.

We report here an extension of this study, employing a variety of cw lasers in a new crossed beam apparatus. After confirming the original experimental results, we sought to investigate the state-to-state dynamics of this reaction by preparing I_2^* in different vibrational–rotational levels of its B state. However, the resulting data could not be reconciled with the LIC mechanism. Rather, we have amassed overwhelming evidence in favor of an LIF origin for the observed metal monoiodide emission. The dependence of emission intensity on laser polarization is therefore considered to apply to the orientation of the reaction product rather than to the orientation of the reagent.

In this paper we present evidence in favor of an LIF mechanism together with new LIF spectra for the $In+I_2$ reaction product. We also demonstrate that a similar interpretation applies to the $Tl+I_2$ system studied previously.

* Present address: Ecole Polytechnique Fédérale de Lausanne, Département de Physique, CH 1007 Lausanne, Switzerland.

0301-0104/81/0000-0000/$02.50

2. Experimental

2.1. General

Fig. 1 presents a schematic drawing of the experimental apparatus in which key elements are lettered for reference purposes. This system consists of two differentially-pumped oven chambers A and a scattering chamber G, each sharing a common liquid nitrogen reservoir. Pumping speeds are such as to allow optimum beam production only for reagents that are efficiently cryopumped at liquid nitrogen temperatures ($\lesssim$77 K). The cw laser light enters and exits via baffle arms which are aligned vertically on an axis passing through the reaction zone N where the two reagent beams cross. Two separate lenses H collect the fluorescence which is detected without dispersion using a photomultiplier or is resolved using a 1 m monochromator K.

2.2. Crossed beam apparatus

The scattering chamber consists of a 50 cm diameter, 50 cm deep, stainless steel cylinder, which is fitted with five 10 cm diameter ports around its circumference at 45° intervals. A rectangular liquid nitrogen reservoir occupies the lower 10 cm of the chamber, which sits above a 3000 l/s oil diffusion pump. The cylinder is sealed at its base against a machined aluminum surface and its top rim against a 2.5 cm thick aluminum lid, using in each case a 0.3 cm thick Viton L-gasket. An ionization gauge is attached to this lid. It monitors the chamber pressure which reaches $\lesssim 10^{-3}$ Pa (10^{-6} Torr) in about 24 h without liquid nitrogen cooling.

The molecular beam apparatus is designed to permit rapid reloading and interchange of beam sources. The two sources, mounted on 15 cm diameter flanges, are suspended from the

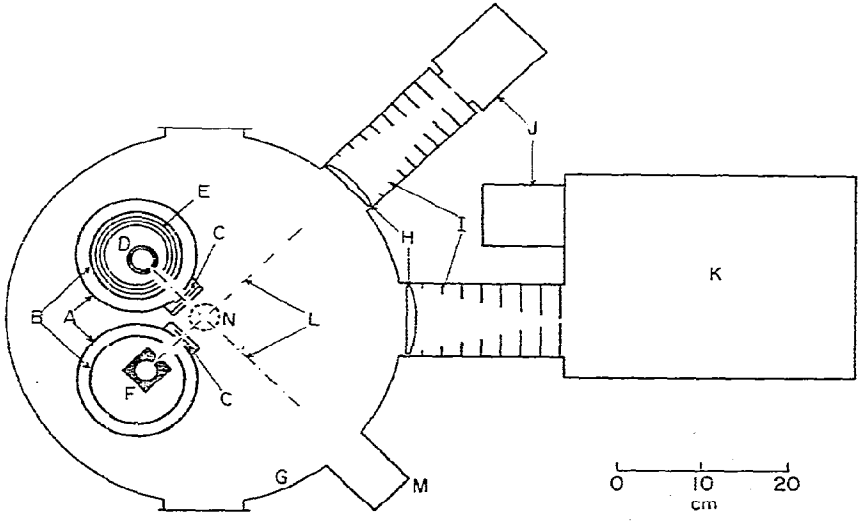

Fig. 1. Cross section of the crossed-beam apparatus: A = differentially-pumped oven chambers; B = water-cooled tube; C = tuning fork choppers; D = high-temperature oven; E = tantalum heat shields; F = iodine oven; G = scattering chamber; H = lenses; I = light baffles; J = cooled photomultipliers; K = 1 m monochromator; L = beam axes; M = port extension to reduce scattered oven light; and N = reaction/excitation zone. Not shown are vertical laser baffle arms that project through the dashed circle.

chamber lid as separate units. Each source chamber A consists of a 50 cm long, 15 cm in diameter nickel–plated copper tube (0.6 cm thick) that passes through the liquid nitrogen reservoir at its lower end and mounts vertically above a baffled 1000 l/s oil diffusion pump. Additionally, each beam source is surrounded by a 10 cm diameter water-cooled nickel–plated copper tube B attached to a supporting flange.

Fig. 2 pictures the metal oven. A high-density graphite oven, sealed by a tapered screw top, is held in the center of the inner copper tube. Three 0.3 cm diameter ceramic posts serve to support it. One of these posts carries, deep into the body of the oven, a W/5% Re to W/26% Re thermocouple that senses the temperature immediately below the 1 mm diameter, 1 mm long oven orifice. The base plate on which the oven is mounted is itself supported by a stainless steel tube that carries water cooling pipes and the thermocouple signal through the top flange via a compression filling. Two micrometer screws acting on this tube allow the metal oven to be fine-positioned during operation.

Three vertical 0.15 cm diameter tungsten hairpin filaments (not shown) heat the metal oven. They draw current in parallel between

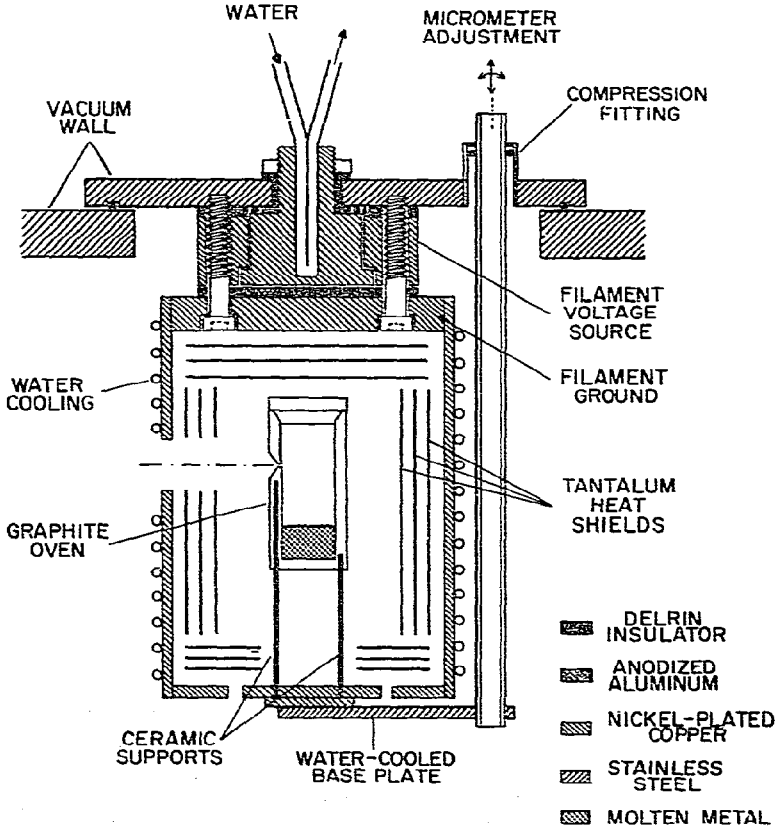

Fig. 2. Cross section of the high-temperature beam source. Not shown are three tungsten hairpin filaments that surround the graphite oven. These filaments are suspended vertically and make electrical contact with the filament voltage source and the filament ground.

two copper electrodes. Spot-welded tantalum sheets provide radiation shielding. Water cooling is applied to the top flange, to the outside of the 10 cm diameter copper tube, and to the oven mount base plate. With clean radiation shields, this oven can attain temperatures $\leq$2200 K.

The metal beam enters the scattering chamber through five sets of tantalum collimating slits. A tuning-fork chopper (Bulova Watch Co.) positioned before the final pair of slits modulates the beam at 400 Hz. The final slit assembly is 1 cm high and 0.4 cm wide. It is located 2.5 cm from the reaction zone and 6.0 cm from the oven orifice.

Indium and thalium oven temperatures of 1700 and 1200 K produced by 2.5 and 1.0 kW input powers, respectively, give beam intensities of about 10^{16} atoms cm^{-2} s^{-1} at the reaction zone. This depletes the oven by approximately 1 g per hour. Under these conditions a typical oven charge of 100 g would last for many runs but the collimating slits require cleaning following each run.

The iodine beam source is suspended from the top flange by a stainless steel tube. A double-chambered stainless-steel oven is employed, having a Teflon gasket seal at the base of the lower chamber for loading. The upper chamber containing the oven orifice is adapted from a 19 mm bellows valve (Veeco). It contains a teflon plug held on a screw thread which permits the lower chamber to be sealed off. Fig. 3 details this mechanism which is vacuum sealed by a stainless-steel bellows. Thus, the I_2 beam can be turned on and off without interrupting the heating of the oven. Without such a seal, the oven would empty in a matter of days if pumped on at room temperature.

Three $\frac{3}{8}$" (9 mm) 500 W cartridge heaters (Chromalox) control the temperature of the upper chamber while three $\frac{1}{4}$" (6 mm) 300 W heaters control that of the lower chamber. Thermistors are connected to both chambers, providing input to separate temperature stabilizers (Thermologic). The temperature of the upper chamber is maintained at least 20 K above that of the lower chamber to prevent

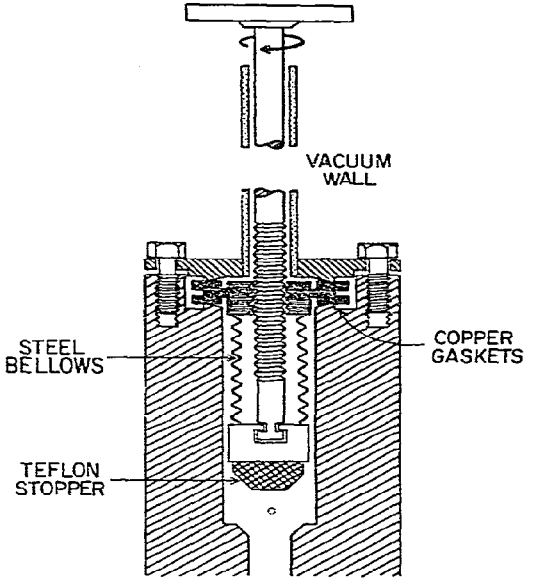

Fig. 3. Cross section of the upper chamber of the iodine oven. Rotation of the handle moves the teflon stopper; when fully down, the lower chamber is sealed.

clogging of the 0.08 cm diameter, 0.16 cm long oven orifice. With a lower chamber temperature of 375 K a beam intensity of about 10^{15} molecules cm^{-2} s^{-1} is obtained in the reaction zone. This beam can also be modulated using the 400 Hz tuning-fork chopper.

The experiments required that the two reagent beams as well as a laser pump beam overlap at the image point of the separate lenses H. The alignment procedure is facilitated by visual observation of fluorescence through the view-ports.

2.3. Excitation and detection optics

Fig. 4 presents a schematic drawing of the optical arrangement employed in this study. Individual lines from either an argon ion laser (Coherent, model CR12) or a krypton ion laser (Spectra-Physics, model 171-01) are used directly in one type of experiment. Alternatively, the output of the argon ion laser is used to pump a home-built linear dye laser

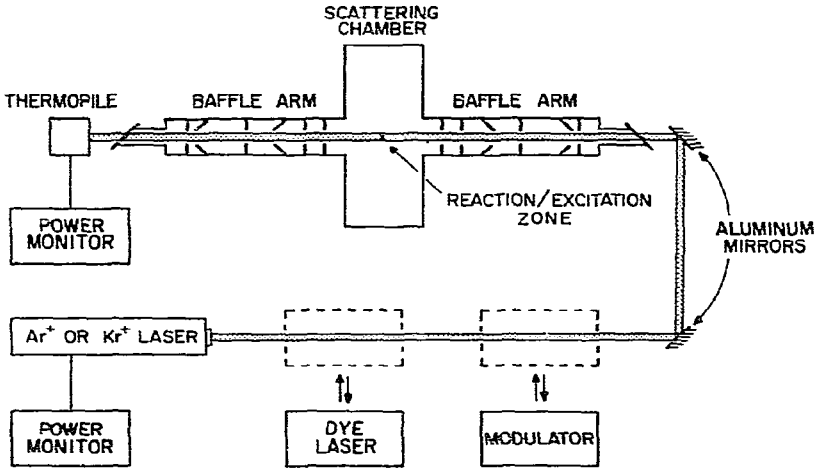

Fig. 4. Schematic drawing of the optical setup. The output of either an argon ion or a krypton ion laser or a dye laser pumped by one of these is directed through the scattering chamber, passing through the reaction/excitation zone.

which has a conventional astigmatic three-mirror cavity [5] and is constructed from components identical to those described elsewhere [6]. A three-plate birefringent filter (Coherent) provides the sole wavelength tuning element, giving a dye laser bandwidth of about 1 cm^{-1}.

In the region 430–480 nm we use a 1.5×10^{-3} M solution of stilbene 420 (Exciton) in a 20:1 mixture of ethylene glycol to methanol; in the region 465–505 nm we use a combination of coumarin 450 and 480 (Exciton) both at 3×10^{-3} M in a 6:1 mixture of ethylene glycol to benzyl alcohol. Both dyes are pumped by the 2.2 W UV lines of the argon ion laser, giving maximum dye laser powers of 270 mW for stilbene and 220 mW for the coumarins.

The laser light sources may be modulated either with respect to intensity using a rotating-blade chopper (PAR model 192) or to linear polarization using a Fresnel rhomb (Karl Lambrecht) [1]. The laser beam is then directed through the scattering chamber by three aluminum mirrors. The baffle arms are similar in design to those employed previously [7]. When measuring the polarization dependence, the Brewster-angled windows on the scattering chamber are replaced by perpendicular ones. The laser power is monitored with a calibrated thermopile (Eppley Laboratories) as it emerges from the second baffle arm.

Two separate 15 cm focal length, 12 cm diameter lenses collect the fluorescence and image it either on a photomultiplier (undispersed fluorescence) or on a 1 m monochromator (Interactive Technology) fitted with a 1200 groove/mm grating blazed at 500 nm and an efficient polarization scrambler†. The degree of linear polarization of the fluorescence can be determined using a rotatable linear sheet polarizer (Polaroid) placed in front of the monochromator entrance slit.

Fluorescence is ultimately detected by a cooled (Centronic, extended S-20 photocathode) photomultiplier. The photomultiplier output feeds either a picoammeter (Keithley model 417) for total photocurrent measurements or a lockin amplifier (PAR model 186A) via a pre-amplifier (PAR model 181) for phase-sensitive detection. Final data are displayed using a two-pen chart recorder.

† This consists of two commercially available (Karl Lambrecht) birefringent wedges held with their faces parallel and their optic axes making an angle of $\pi/4$.

3. Results

3.1. $In+I_2$

The fluorescence spectrum resulting from illumination of the reaction zone with the 8 W output of the 514.5 nm line of the argon ion laser is shown in fig. 5a. This spectrum was obtained under crossed beam conditions using phase-sensitive detection referenced to the modulation of the indium beam. The scan speed was 5 nm/min; the spectrum was recorded with 0.5 nm resolution and a 1 s time constant. The maximum signal levels were $\approx 10^{-10}$ A. The sharp spikes to the red of the pump wavelength are caused by interference from I_2 fluorescence. Fig. 5b shows the corresponding spectrum obtained with the 5 W output of the 488.0 nm line of the argon ion laser. This spectrum is taken under identical conditions as that of fig. 5a except that a longer time constant (3 s) and a slightly poorer resolution ($\approx$0.7 nm) were employed. It is well known that this wavelength photodissociates I_2, accounting for the absence of I_2 LIF interference to the red of the laser pump wavelength in fig. 5b. Fig. 6 displays spectra recorded using two lines of the krypton ion laser, specifically the 1.8 W, 568.2 nm line and the 0.5 W, 530.9 nm line. The time constant was 3 s and the resolution was 1.0 nm.

In another experiment a heated Brewster-angled cell containing I_2 vapor was placed inside the cavity of the argon ion laser while operating on the 514.5 nm line. This reduced the laser power by 25% while preventing laser action on those modes absorbed by I_2, thereby producing two $\approx$1 GHz holes in the $\approx$8 GHz wide laser line profile. The resulting laser output pumped I_2 in an extracavity glass cell with $\leq$1% of its previous efficiency [9] and pumped the (Doppler-free) I_2 beam so weakly that I_2 fluorescence could not be recorded. Spectra taken for the $In+I_2$ reaction with and without this intracavity I_2 absorption cell were indistinguishable; moreover, they were essentially identical to that shown in fig. 5a. Fig. 7 shows the normalized ratio of intensities for representative peaks in this spectrum recorded with and without the intracavity cell.

The spectra shown in figs. 5 and 6 appear to "hug" the pump wavelength, which is characteristic of an LIF process. Furthermore, the signals obtained are *not* dependent on producing I_2^*. Consequently, we were forced to abandon the previously proposed LIC mechanism in favor of an LIF origin for the signal. To test

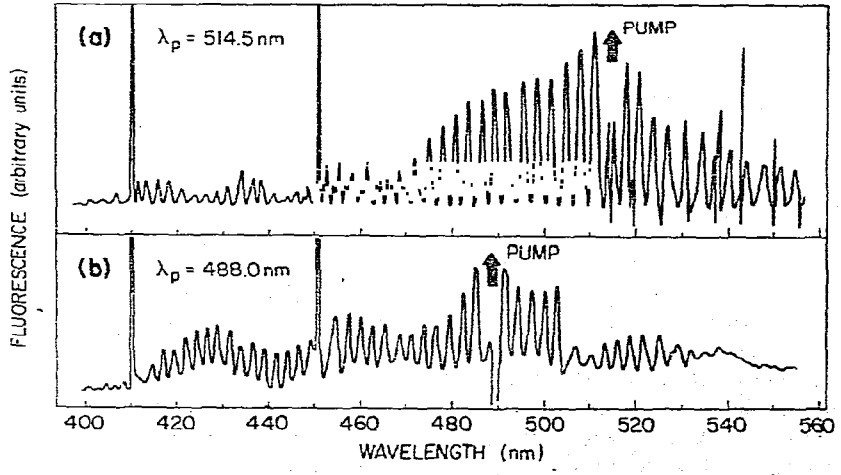

Fig. 5. Fluorescence spectra resulting from illumination of the $In+I_2$ reaction zone with an argon ion laser at a wavelength of (a) 514.5 nm or (b) 488.0 nm under identical crossed-beam conditions. Arrows mark these pump wavelengths.

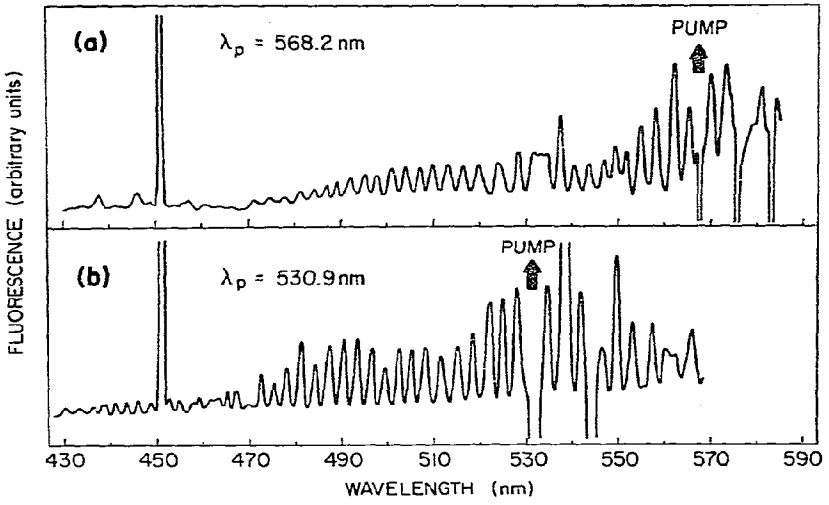

Fig. 6. Fluorescence spectra resulting from illumination of the $In+I_2$ reaction zone with a krypton ion laser at (a) 568.2 nm and (b) 530.9 nm under identical crossed-beam conditions to those of fig. 5.

further this hypothesis, LIF excitation spectra were recorded by scanning the laser wavelength while collecting the undispersed fluorescence. Fig. 8 shows a 2.5 nm/min scan of the 430–500 nm region, taken using an In-beam–I_2-gas scattering arrangement. Replacement of the I_2 beam by a bulk gas served to increase signals by an order of magnitude, considerably improving the signal-to-noise ratio of these data. The observation direction was perpendicular to both the laser and In beams (see fig. 1). This geometry minimized the scattered oven light that constitutes a signal $\approx 10^{-8}$ A compared to InI LIF signals $\approx 10^{-7}$ A and scattered laser light $\approx 10^{-11}$ A. The lock-in amplifier was referenced in this case to modulation of the laser beam (400 Hz) and a 1 s time constant was employed. The spectrum was obtained using the

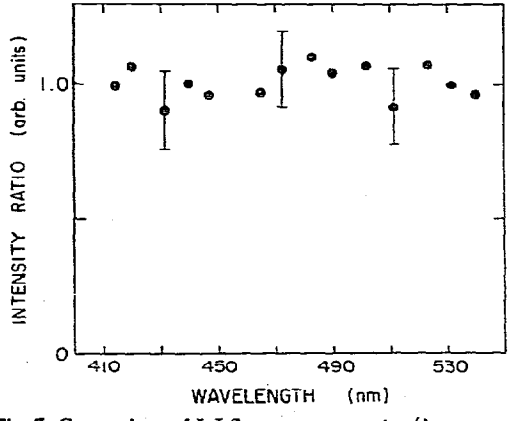

Fig. 7. Comparison of InI fluorescence spectra (λ_p = 514.5 nm) recorded with and without an I_2 cell inside the argon ion laser cavity. Ratios of intensities for representative peaks in the two spectra are shown together with the wavelength. Typical error bars are also indicated.

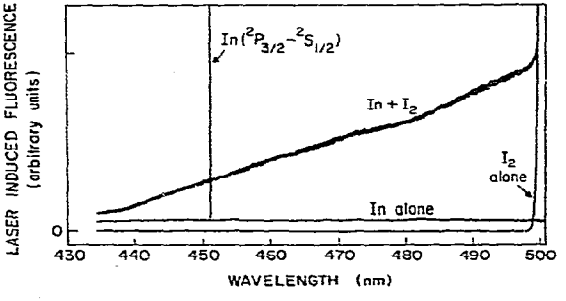

Fig. 8. Laser-induced fluorescence spectra of the reagents alone and the products of the $In+I_2$ reaction under beam-gas conditions. The laser scan speed is 2.5 nm/min with a 1 s output time constant. The spectra have been corrected for variation in laser power with wavelength.

overlapping dye range described in section 2.3. Although the spectrum was corrected for the intensity variation of the probe laser, no allowance was made however for the (small) variation of the S-20 photocathode response with fluorescence wavelength as a function of excitation wavelength. By scanning a factor of ten more slowly, individual rotational band head profiles could be discerned, as shown in fig. 9. LIF intensities were found to be linear with I_2 pressure up to 0.1 Pa (10^{-4} Torr), the maximum pressure employed.

A laser-induced fluorescence signal was observed from either reagent alone. The I_2 fluorescence prevented InI excitation spectra from being recorded to the red of 500 nm (see fig. 8). The fluorescence from the In beam consisted of two atomic lines at 451.1 nm ($In\ ^2P_{3/2}-^2S_{1/2}$) and at 410.2 nm ($In\ ^2P_{1/2}-^2S_{1/2}$) of equal intensity (see fig. 5). The contribution of this fluorescence to the total fluorescence under typical working conditions is shown in fig. 8. The intensity of the atomic In lines increased with indium oven temperature more rapidly than did the atomic indium beam flux, as monitored by tuning the laser to the 451.1 nm line. The optimum signal-to-noise level was obtained with an oven temperature of 1610 K.

We have not been able to establish unequivocally the origin of this fluorescence. At first it was thought that an impurity, either an oven contaminant or a low pressure gas in the scattering chamber, was responsible for the observed atomic indium fluorescence. We imagined that indium atoms reacted with the impurity to produce a species that was subsequently photodissociated by the laser to yield excited indium atoms in the $^2S_{1/2}$ state. However, the use of the highest purity indium metal available (99.999%, Apache Chemicals) and the observation that the atomic fluorescence was not related to the ambient pressure in the scattering chamber argued against this possibility.

The strong dependence on oven temperature may suggest a mechanism involving indium dimers. A single photon from the laser pump light has insufficient energy to produce In ($^2S_{1/2}$) photofragments from ground state In_2. Instead we postulate that the indium dimers are electronically excited by the oven light [9] and that these species are then photodissociated by the laser to produce excited indium atoms. The blackbody radiation from the In oven is rather intense; we have even been able to observe weak I_2 fluorescence induced by the oven light when the In beam is so directed as to miss entering the scattering chamber. We estimate that at $\approx$1700 K the indium oven provides $\geq$10 mW of light bluer than 500 nm. Since excited dimers present in the beam at a level of

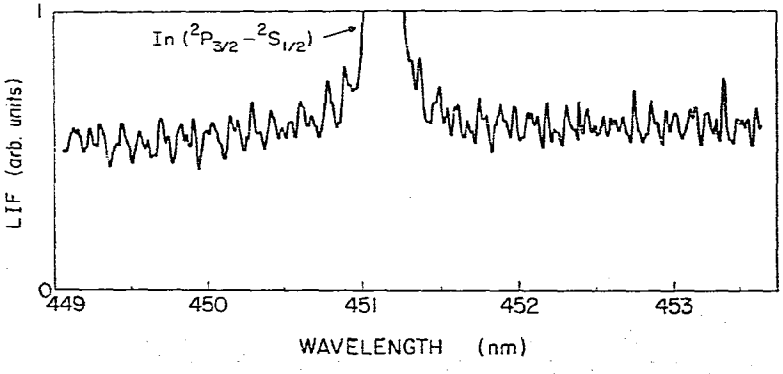

Fig. 9. Laser-induced fluorescence spectrum of the nascent InI product from the beam-gas reaction $In + I_2$. The noise on the spectrum is much less than the structured features which are fully reproducible. The laser scan speed is 0.25 nm/min with a 1 s output time constant. No correction has been made for the (small) variation of laser power with wavelength.

one part in ten million would account for the effect, absorption of a small fraction of this light by the 1% or so of dimers in the beam would be sufficient.

The polarization of the InI fluorescence was determined using a beam-gas scattering setup in which the pump beam is at right angles to the observation direction. This configuration is the same as that used previously [1] and again provides about an order of magnitude more signal than when an I_2 cross beam is employed. The degree of linear polarization, P, is defined as $P=(I_\parallel-I_\perp)/(I_\parallel+I_\perp)$, where $I_\parallel$ and $I_\perp$ refer to the signal intensities with a polarization analyzer parallel to and perpendicular to the fixed polarization vector of the laser pump beam, respectively. We recorded a polarization of $P=12\pm2\%$ of the fluorescence at 501.5 nm using a 0.5 W pump beam at 514.5 nm. Upon increasing the power of the pump beam to 8 W, the degree of polarization decreases to about 7%, due to optical pumping [10].

An alternative method of measuring the polarization is to rotate the polarization vector of the laser beam. Here one determines the ratio $p=[I(\parallel)-I(\perp)]/[I(\parallel)+I(\perp)]$, where $I(\parallel)$ and $I(\perp)$ refer to the signal intensities with the laser polarization vector parallel to and perpendicular to the observation direction, respectively. A simple analysis shows that $I(\parallel)=I_\parallel+I_\perp$ while $I(\perp)=2I_\perp$; hence $p=-P/(2-P)$ and for small values of P, the value of p is about half that of P. Our measurements were consistent with the above. We did not concentrate our efforts on this alternative method because not only is it less sensitive, but also more prone to measurement artifacts.

3.2. $Tl+I_2$

Having established the origin of the InI emission in the $In+I_2$ reaction to be laser-induced fluorescence, we suspected that a similar explanation might pertain to the previously studied $Tl+I_2$ reaction system. We checked this hypothesis by searching for TlI emission in the absence of I_2 pumping. Fig. 10 shows the resulting spectra when the pump laser is tuned to 514.5 nm (fig. 10a) or 480.0 nm (fig. 10b). These spectra were recorded under essentially the same conditions as in fig. 5.

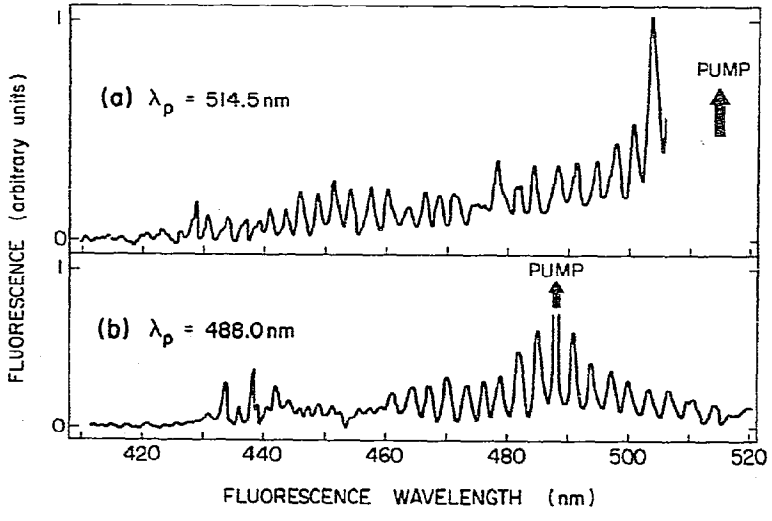

Fig. 10. Fluorescence spectra resulting from illumination of the $Tl+I_2$ reaction zone with an argon ion laser at (a) 514.5 nm and (b) 488.0 nm under essentially identical conditions to fig. 5.

Again we observed in the case of 515.4 nm pumping coincidental I_2 fluorescence (not shown in fig. 10a) as well as in both cases laser-induced fluorescence of TlI formed in the ground state reaction $Tl+I_2 \rightarrow TlI+I$. Because the spectroscopy of TlI is not as well developed as even that of InI, we did not pursue further the study of the $Tl+I_2$ reaction system.

4. Discussion

We have obtained strong LIF signals, S_{LIF}, from the $In+I_2$ reaction products throughout the visible, whereas pumping of the I_2 reagent failed to produce detectable LIC signals, S_{LIC}. Comparing InI emission signals obtained with and without I_2 pumping by the 514.5 nm laser light, we estimate the signal ratio for these two reaction mechanisms to be

$$S_{LIF}/S_{LIC} \geq 100. \tag{1}$$

In section 4.1, we derive an analytical approximation for this signal ratio in terms of the relevant reactive cross sections for these two processes; in section 4.2, we use the inequality given in eq. (1) to place an upper bound on σ_{LIC}, the cross section for the LIC reaction; and in section 4.3, we discuss the nature of the nascent InI product formed in the $In+I_2$ reaction.

4.1. Comparison of laser induced fluorescence and laser induced chemiluminescence reaction rates

Let us consider the reaction $A+BC \rightarrow AB(v'', J'')+C$ in which the AB product is detected by LIF. The magnitude of S_{LIF} will depend on the following processes under single-collision conditions:

reaction:	$A_i+BC_i \rightarrow AB_i(v'', J'')+C_i$,	(2a)
ground state fly out:	$AB_i(v'', J'') \rightarrow AB_o(v'', J'')$,	(2b)
absorption:	$AB_i(v'', J'')+h\nu \rightarrow AB_i(v', J')$,	(2c)
emission:	$AB_i(v', J') \rightarrow AB_i(v, J)+h\nu$,	(2d)
excited state fly out:	$AB_i(v', J') \rightarrow AB_o(v', J')$.	(2e)

In eq. (2) the subscripts i and o indicate species in and out of the reaction/ excitation zone of radius R, which is assumed to be homogeneously illuminated by the probe laser. The observation zone is taken to be smaller than or equal to this region which encompasses the former.

Assuming that in this cw experiment all species reach steady-state concentrations, then we can write

$$[AB_i(v'', J'')] = \frac{[A_i][BC_i]\sigma_{LIF}(AB; v'', J'')\bar{V}(A, BC)}{\bar{V}(AB)/R + I(\nu)\varepsilon(AB; \nu)}, \tag{3}$$

where $\sigma_{LIF}(AB; v'', J'')$ is the (phenomenological) cross section for producing AB products in the vibration–rotation state (v'', J'') which is pumped by the laser of intensity $I(\nu)$ at frequency ν and which has an absorption cross section denoted by $\varepsilon(AB; \nu)$. In eq. (3) $\bar{V}(A, BC)$ is the mean center-of-mass velocity of the reagents, $\bar{V}(AB)$ is the mean laboratory velocity of the AB product, and we have assumed step function behavior for the various spatial distributions rather than more realistic (e.g., gaussian) profiles.

We also find that

$$[AB_i(v', J')] = \frac{[AB_i(v'', J'')]I(\nu)\varepsilon(AB; \nu)}{\bar{V}(AB)/R + 1/\tau(AB; v', J')}, \tag{4}$$

where $\tau(AB; v', J')$ is the radiative lifetime of the $AB(v', J')$ molecule. We may then write the LIF signal as

$$S_{LIF} = d[AB_i(v', J')]/\tau(AB; v', J'), \tag{5}$$

where d is the fluorescence detection efficiency. Substitution of eqs. (3) and (4) into (5) yields the expression

$$S_{LIF} = \frac{d[A_i][BC_i]\sigma_{LIF}(AB; v'', J'')\bar{V}(A, BC)I(\nu)\varepsilon(AB; \nu)}{\tau(AB; v', J')[V(AB)/R + 1/\tau(AB; v', J')][\bar{V}(AB)/R + I(\nu)\varepsilon(AB; \nu)]}. \tag{6}$$

We consider next the rival laser-induced reaction $A + BC^* \rightarrow AB^* + C$ in which the chemiluminescence of the AB^* product is detected. The magnitude of S_{LIC} will depend on the following processes under single-collision conditions:

absorption:	$BC_i(v'', J'') + h\nu \rightarrow BC_i^*$,	(7a)
reagent fly out:	$BC_i^* \rightarrow BC_o^*$,	(7b)
reagent emission:	$BC_i^* \rightarrow BC_i + h\nu$,	(7c)
reaction:	$A_i + BC_i^* \rightarrow AB_i^* + C_i$,	(7d)
product fly out:	$AB_i^* \rightarrow AB_o^*$,	(7e)
product emission:	$BC_i^* \rightarrow BC_i + h\nu$	(7f)

In a similar manner we find

$$[BC_i^*] = \frac{[BC_i(v'', J'')]I(\nu)\varepsilon(BC; \nu)}{\bar{V}(BC^*)/R + 1/\tau(BC^*) + [A_i]\sigma_{LIC}(BC^*)\bar{V}(A, BC^*)}, \tag{8}$$

where all symbols are defined in an analogous manner. It follows that

$$[AB_i^*] = \frac{[A_i][BC_i^*]\sigma_{LIC}(BC^*)\bar{V}(A, BC^*)}{\bar{V}(AB^*)/R + 1/\tau(AB^*)} \tag{9}$$

and hence

$$S_{LIC} = \frac{d[A_i][BC_i(v'', J'')]\sigma_{LIC}(BC^*)\bar{V}(A, BC^*)I(\nu)\varepsilon(BC; \nu)}{\tau(AB^*)[\bar{V}(AB^*)/R + 1/\tau(AB^*)][\bar{V}(BC^*)/R + 1/\tau(BC^*) + [A_i]\sigma_{LIC}(BC^*)\bar{V}(A, BC^*)]}. \tag{10}$$

Using eqs. (6) and (10) we obtain the signal ratio

$$S_{LIF}/S_{LIC} = [\sigma_{LIF}(AB; v'', J'')/\sigma_{LIC}(BC^*)]\{[BC_i]/[BC_i(v'', J'')]\}$$
$$\times \varepsilon(AB; \nu)/\varepsilon(BC; \nu)\left\{\frac{\bar{V}(BC^*)/R + 1/\tau(BC^*) + [A_i]\sigma_{LIC}(BC^*)\bar{V}(A, BC^*)}{\bar{V}(AB)/R + I(\nu)\varepsilon(AB; \nu)}\right\}. \tag{11}$$

One expects the fly out rate to exceed the rate of reaction or the pump rate. Then eq. (11) reduces to

$$S_{LIF}/S_{LIC} = [\sigma_{LIF}(AB; v'', J'')/\sigma_{LIC}(BC^*)]\{[BC_i]/[BC_i(v'', J'')]\}$$
$$\times [\varepsilon(AB; \nu)/\varepsilon(BC; \nu)]\{[\bar{V}(BC^*)/R + 1/\tau(BC^*)]/[\bar{V}(AB)/R]\}. \tag{12}$$

As expected, the S_{LIF}/S_{LIC} ratio depends on the ratio of the cross sections for the respective processes and the absorption coefficients of the species that are pumped by the laser. In addition S_{LIF}/S_{LIC} depends on the ratio of all BC reagents to those BC reagents in a set of quantum states pumped by the laser. Finally, S_{LIF}/S_{LIC} depends on the ratio of the decay rate of BC^* product (by fly

out and by emission) to the decay rate of the AB product (by fly out). For strongly allowed transitions, the last factor will be much larger than unity. Consequently, LIF detection is often expected to dominate LIC detection when both processes occur.

4.2. Upper bound for the $In + I_2^*$ reaction cross section

The 514.5 nm laser light pumps the P(13) and R(15) lines of the (43, 0) band of the $I_2B\,^3\Pi(0_u^+)$–$^1\Sigma(0_g^+)$ system. For a 400 K effusive beam of I_2, we estimate that $[I_2]/\{[I_2(0, 12)]+[I_2(0, 16)]\}$ is ≈ 250 and for $\tau(I_2^*)$ we take ≈ 2.5 μs [11]. The InI product can absorb in the visible on both the $B\,^3\Pi_1$–$X\,^1\Sigma_0^+$ and the $A\,^3\Pi_0$–$X\,^1\Sigma_0^+$ transitions [12, 13]. Schwenz et al. [14] have estimated radiative lifetimes of the indium monohalide $^3\Pi$ states to be 2.4 μs, from which we will assume $\varepsilon(\mathrm{InI}; \nu)/\varepsilon(I_2; \nu)$ is on the order of unity. We further assume that Δv ranges from −10 to +10. We calculate from available spectroscopic data [11, 12] that the vibrational levels $v'' \approx 43$–49 of the B–X system and $v'' \approx 53$–55 of the A–X system may absorb the 514.5 nm laser line. By analogy with the $Tl + I_2$ reaction [2], the total cross section for the $In + I_2$ reaction is expected to be about $\approx 10^{-14}\,\mathrm{cm}^2$. We suppose that an average two of the four hundred or so accessible rotational levels absorb; hence we estimate that $\sigma_{\mathrm{LIF}}(\mathrm{InI}; v'', J'') \approx 10^{-17}\,\mathrm{cm}^2$.

Production of these high vibration–rotation levels of InI accounts for approximately half of the reaction exoergicity of 175 kJ mol^{-1}. If the remaining energy is equipartitioned between translation and rotation, then $\bar{V}(\mathrm{InI})$ is about 200 ms^{-1}. For our excitation/reaction zone of radius $\approx 4 \times 10^{-3}$ m, $\bar{V}(\mathrm{InI})/R$ is $\approx 5 \times 10^4\,\mathrm{s}^{-1}$. For an effusive beam at 400 K, $\bar{V}(I_2)$ is also $\approx 200\,\mathrm{ms}^{-1}$ so that $\bar{V}(\mathrm{InI})/\bar{V}(I_2^*) \approx 1$.

Substituting eq. (1) and the above numerical values into eq. (12), we obtain the result

$$\sigma_{\mathrm{LIC}}(\mathrm{InI}^*) \leq 2.5 \times 10^{-16}\,\mathrm{cm}^2. \tag{13}$$

Assuming that the total reaction cross section for $In + I_2^*$ is at least as large as for $In + I_2$, the branching ratio for the production of chemiluminescent products is ≤2.5%. We conclude that even for a laser induced chemiluminescence cross section of several square ångstroms, the interference from laser induced fluorescence masks the existence of the former process. It is interesting to note that the chemiluminescent reaction $In + F_2 \rightarrow InF^* + F$ which has a reaction exothermicity comparable to $In + I_2^*$ is reported [14] to have an absolute chemiluminescent cross section of $\approx 5 \times 10^{-18}\,\mathrm{cm}^2$.

4.3. Characterization of the InI product

No attempt has been made to extract detailed product state distributions from the excitation spectra obtained. Too little is known presently about the spectroscopy of InI, particularly for highly excited states. Furthermore, it is apparent from fig. 8 that (1) the vibrational bands of the A–X and B–X electronic systems of InI overlap severely, and (2) we have nowhere near the resolution necessary to observe individual rotational features. Nevertheless, it is clear that a large fraction of the total energy appears at InI vibrational energy. At thermal energies absorption maxima occur for $\Delta v \approx 0$ in both the A–X and B–X band systems [12]. Assuming that this trend continues to high vibrational levels, i.e., that the $\Delta v \approx 0$ sequence dominates, we can conclude that an inverted vibrational population distribution of InI is produced, peaking at $v'' \geq 50$. This implies that the average fraction of total energy going into vibration, $\langle f_v \rangle$, is greater than or equal to 0.5. The high level of vibrational excitation suggests a direct mechanism with early release of the excess energy of reaction. By contrast, for a reaction proceeding through a long-lived complex, one would expect a maximum population in $v'' = 0$. The analogous reactions of B and Al with F_2 are also thought to produce vibrational population inversions [15] as do the chemiluminescent reactions of In and Ga with F_2 [14].

The observed degree of linear polarization of the InI fluorescence, $P \approx 12 \pm 2\%$, is in good agreement with that recorced previously [1]. However, we now believe that this polarization refers to the rotational polarization of the product molecules for these LIF experiments [16]. Because the excitation spectrum is an overlap of the $A\,^3\Pi_0$–$X\,^1\Sigma_0^+$ and the $B\,^3\Pi_1$–$X\,^1\Sigma_0^+$ band systems, interpretation of this polarization measurement is not possible without a detailed identification of the resonance fluorescence branches that contribute to the observed signal and a knowledge of their individual intensities.

Acknowledgement

This work was supported by Air Force Office of Scientific Research under AFOSR 77-3363. of Scientific Research under AFOSR 77-3363 and AFOSR 81-0053.

References

[1] R.C. Estler and R.N. Zare, J. Am. Chem. Soc. 100 (1978) 1323.
[2] A. Geldeon, S.A. Edelstein and P. Davidovits, J. Chem. Phys. 55 (1971) 5171.
[3] R.N. Zare and P.J. Dagdigian, Science 185 (1974) 739.
[4] J.L. Kinsey, Ann. Rev. Phys. Chem. 28 (1977) 349.
[5] R.L. Kohn, C.V. Shank, E.P. Ippen and A. Dienes, Opt. Commun. 3 (1971) 177.
[6] C.R. Webster, L. Wöste and R.N. Zare, Opt. Commun. 35 (1980) 435.
[7] (a) J.G. Pruett and R.N. Zare, J. Chem. Phys. 64 (1976) 774;
(b) L. Stein, J. Wanner and H. Walther, J. Chem. Phys. 72 (1980) 1128.
[8] R.N. Zare, Sci. Am. 236 (1977) 86 (fig. 1).
[9] D.S. Ginter, M.L. Ginter and K.K. Innes, J. Phys. Chem. 69 (1965) 2480.
[10] R.E. Drullinger and R.N. Zare, J. Chem. Phys. 51 (1969) 5538; 59 (1973) 4225.
[11] L. Brewer and J. Tellinghuisen; J. Chem. Phys. 56 (1972) 3929.
[12] (a) M. Wehrli and E. Miescher, Helv. Phys. Acta. 7 (1934) 298.
(b) M. Wehrli, Helv. Phys. Acta 7 (1934) 611.
[13] (a) S. P. Vaidya, Ph.D. Thesis, University of Baroda (1979).
(b) A.B. Darji and S.P. Vaidya, Curr. Sci. 46 (1977) 486.
[14] R.W. Schwenz, L.C. Geigerland and J.M. Parson, J. Chem. Phys., submitted for publication.
[15] W.W. Rice, W.M. Beatie, R.C. Oldenborg, S.E. Johnson and P.B. Scott, Appl. Phys. Letters 28 (1976) 444.
[16] D.A. Case, G.M. McClelland and D.R. Herschbach, Mol. Phys. 35 (1978) 541.